Nanoscale

Accepted Manuscript

This article can be cited before page numbers have been issued, to do this please use: X. Chen, Y. Ren, L. Hou, X. Feng, T. Jiang and H. Jiang, *Nanoscale*, 2019, DOI: 10.1039/C8NR09148J.

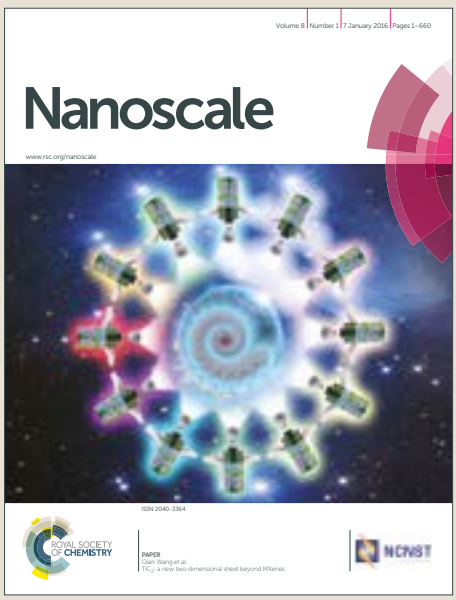

ROYAL SOCIETY OF CHEMISTRY

rsc.li/nanoscale

View Article Online
DOI: 10.1039/C8NR09148J

Journal Name

ARTICLE

Induced Charge Electro-osmotic Particle Separation

Xiaoming Chen[a], Yukun Ren*[a,b,c], Likai Hou[a], Xiangsong Feng[a], Tianyi Jiang[a], and Hongyuan Jiang*[a,b]

Received 00th January 20xx,
Accepted 00th January 20xx

DOI: 10.1039/x0xx00000x

www.rsc.org/

Vortex-based separation is a promising method in particle-particle separation and has only been demonstrated theoretically some years ago. To date, a continuous-flow separation device based on vortices has not been conceived because many known vortices were either unstable or controlling them lacked precision. Electro-convection from induced charged electro-osmosis (ICEO) has advantages, such as adjustable flow profile, long-range actuation, and long-lived vortices, that offers an alternative means of particle separation. We found though a different ICEO focusing behaviour of particles whereby particles were trapped and concentrated in two vortex cores. Encouraged by these features of ICEO vortices, we proposed a direct method for particle separation in continuous flows. In various experiments, we first characterized the ICEO-induced focusing performances of various kinds of particle samples in a straight channel embedded with an individual central bipolar electrode, presenting a justifiable explanation. Second, the combined dependences of ICEO particle separation on sample size and mass density were investigated. Third, an application to cell purification was performed in which we obtained a purity surpassing 98%. Finally, we investigated the ICEO characteristics of nanoparticles, exploiting our method in isolating nanoscale objects by separating 500-nm and 5-μm polystyrene beads, gaining clear separation. Certain features of this method, such as easy-operation, simple-structure, prefocusing-free, continuous-flow, physical property-based, indicate a good potential in tackling environmental monitoring, cell sorting, chemical analysis, isolation of uniform-size graphene and transesterification of micro-algal lipids to biodiesel.

Introduction

Particle separation is an essential process prior to water quality analysis[1], nanoscale exosomes isolation[2, 3], early-stage cancer diagnosis[4], uniform-size (microscale or nanoscale) graphene isolation[5, 6], the transesterification of microalgal lipids to biodiesel[7] and so on[8]. For such purposes, many effective methods of separation have been developed, including acoustic waves[4, 9], dielectrophoresis (DEP)[10-12], magnetism[7, 13], optical field[14, 15], and centrifugation[16]. Although each method has its specific advantages, each is also limited by natural drawbacks. For instance, acoustic separation is an attractive method of separation that can deal with many tricky issues involving isolating circulating tumour cells from white blood cells[4] and exosomes from whole blood[2]. However, to focus the particles into a stream, this method depends on sheath flow involving complex operations that encumbers the device with a peripheral system to control and drive the many fluids. Centrifugation may also achieve massive particle separation; the high-speed rotation makes it near impossible to integrate it with other platforms[16]. Furthermore, magnetism offers excellent performance in a separation device, but is only suitable for magnetic particles or particles able to be magnetically labelled[7, 13]. Moreover, many DEP-based separation devices, aside from suffering the same issue as acoustic separation devices, are unable to avoid the adherent growth of cells or adhesion of particles on the electrodes[11]. Therefore, a more effective and simple method of separation of particles is required.

Many scientists have discovered that light particles in vortices do not simply follow local streamlines but are drawn into vortices, thereby enabling particle trapping[17, 18]. However, this mechanism fails for heavy particles as one would expect that, sooner or later, any individual particle is pushed out of a vortex into the flow field, and escape[18]. These two distinct particle behaviours in vortices throw light on the design of a vortex-based approach to particle separation. Indeed, the idea that vortices may be used in particle–particle separators had been posited and validated theoretically[18, 19]. More importantly, the vortex-based method of particle separation has many merits, such as being based on the physical properties of particles, having ease of operation, and being a contact-free process. However, to the best of our knowledge, a continuous-flow separation device based on vortices has rarely been considered because many known vortices are either unsteady or not precisely controllable. Motivated by these considerations, we looked for an effective method to generate steady, long-lived, controllable, and reproducible vortices in our vortex-based separator design.

Recently, induced-charge electro-osmosis (ICEO) has received considerable attention for vortex generation[20, 21],

[a] School of Mechatronics Engineering, Harbin Institute of Technology, Harbin 150001, PR China. E-mail: rykhit@hit.edu.cn
[b] State Key Laboratory of Robotics and System, Harbin Institute of Technology, Harbin 150001, PR China. E-mail: jhy_hit@hit.edu.cn
[c] State Key Laboratory of Nonlinear Mechanics, Chinese Academy of Sciences, Beijing 100190, PR China.
Electronic Supplementary Information (ESI) available: See DOI: 10.1039/x0xx00000x

View Article Online
DOI: 10.1039/C8NR09181

which arises from the action of an external electric field on ionic charges induced around a polarizable surface[22]. Immediately after an AC signal is applied, an electric field is set up with field lines intersecting the electrode at right angles. In response to the applied fields, the positive ions are driven towards a charge cloud on one side of the electrode, whereas the negative ions are driven to the other, inducing an equal and opposite surface charge on the electrode[22]. The normal electric field injects the ions into a charge cloud to charge an induced double layer (IDL). Over a characteristic RC charge relaxation time, the IDL reaches a steady state and becomes an ideal insulator by screening the normal electric field[20]. Under this scenario, the tangential electric field component exerts a body force on the electrically charged fluid in the screening cloud, accelerating the ions and fluid. The resulting electro-osmotic fluid flow appears to 'slip' just outside the screening layer[22]. Furthermore, the ICEO flow near the electrode surface creates vortices from the bulk fluid flow. In particular, for a symmetric channel configuration, a pair of symmetrical ICEO vortices are created around an oppositely charged central floating electrode. In addition, the vortex profile can be adjusted by varying the external field[22]. Therefore, for the design of a vortex-based separator, exploiting these ICEO vortices may in practice be feasible.

We found in our previous experiment[17] that heavy particles do escape from the ICEO vortices and are pushed towards the flow stagnation line (FSL) by a transverse flow near the floating electrode. The countering upward drag from the fluid flow and a downward-pushing gravitational effect gives rise to a stable focused particle stream in the FSL[17]. With this as a basis, many microfluidic techniques have been developed to manipulate micro-samples, including scale particle focusing[23], single particle trapping[24], and sample concentrating/directing[25]. Interestingly, a different particle-focusing behaviour of ICEO was found recently in which the ICEO vortices have sufficient strength to overcome the gravitational effect. The particles are then promoted to a higher level and are captured by the vortices, whirling around the vortex cores on both sides of the floating electrode. This non-negligible effect of the DEP force and gravity gives rise to two attractors at the two vortex cores[19] that reduce the closed orbits of these particles and entrap them. Consequently, these particles are focused into a fine particle stream on both sides of the floating electrode. Moreover, after systematic experiments, we found that the location of the focus of some particles can be switched quite flexibly from the FSL to the vortex cores or vice versa by an easy adjustment of the voltage frequency and intensity. Enthused by these aspects, we exploited these two different particle-focusing characteristics of ICEO to separate mixed particles. Surprisingly, the ICEO vortices performed wonderfully well in particle separation. To date, this method of particle separation based on ICEO vortices has not been studied before. Significantly, aside from the aforementioned advantages of the vortex-based method of separation, ICEO flow also has many advantages, such as long-range actuation[26], long-lived vortices, precise external field control[22], and a gentle operational environment[22]. An investigation of these aspects needed to be conducted.

Herein, we describe an ICEO-vortex-based platform that isolates directly targeted particles from a mixture. This ICEO-vortex-based, automated, point-of-care system achieves single-step and on-chip extraction of nano/micro objects from mixtures, bypassing prefocusing preparations. In addition, conditions for a gentle separation exist under low external voltages, which are often preferable in real devices[22]. First, we designed and fabricated the ICEO separator and configured a corresponding physical model that coupled a flow and an electric field. Second, we conducted systematic series of experiments to test and validate the microfluidic chip by separating 5-µm polystyrene (PS5) and 4-µm silica micro-beads. The outcomes were in good agreement with our theoretical predictions. Third, we further explored the capabilities of this device for density- and size-based particle separation. Fourth, we employed this method to purify cells, obtaining a purity that exceeds 98%. Finally, we investigated the ICEO characteristics of nanoparticles, and put our method to isolate nanoscale objects[2, 3] by separating 500-nm and PS5 beads and found a reliable separation. The main advantages of this method, such as ease of integration, a contact-free separation condition, a gentle operation environment, a prefocusing-free process, enable the method to be a potential alternative in disease diagnosis, environmental monitoring, isolation of uniform-size graphene, and chemical analysis.

Materials and Methods

Device design and fabrication.

A glass slide coated with thin transparent indium tin oxide (ITO) material (Zhuhai, Guangdong, China) served as a substrate for the device. The patterned ITO-based electrode including left and right driving electrodes, and floating electrode, was designed using AutoCAD software and fabricated using two consecutive steps: standard soft photolithography and etching. The PDMS-based channel fabrication included two continuous processing steps: patterning the microchannel mould and casting the PDMS. Briefly, a two-layer negative dry film with a thickness of 35 µm (Riston SD238, Dupont, USA) was employed as a mould for the PDMS-based channel, which was patterned to a pre-designed structure through standard soft photolithography. To reduce the damage to the PDMS channel during demoulding, the mould was vapour coated in advance with 1H, 1H, 2H, 2H-perfluorooctyltrichlorosilane (Sigma Aldrich, USA) to reduce its surface energy. Then, Sylgard 184 Silicone Elastomer Base and Sylgard 184 Silicone Elastomer Curing Agent (Dow Corning, USA) were mixed at a 10:1 (weight: weight) ratio and cast with the dry-film mould. The PDMS-based micro-channel was aligned and bonded to the substrate and ITO-based electrode after a surface treatment with oxygen plasma. Further details of the fabrication process may be found in our previous work[10, 17].

Device operation.

The ICEO-vortex-based particle separation device was mounted on the platform of an optical microscope (BX53, Olympus, Japan). The trajectories of the particles in the device were

View Article Online
DOI: 10.1039/C8NR09148J

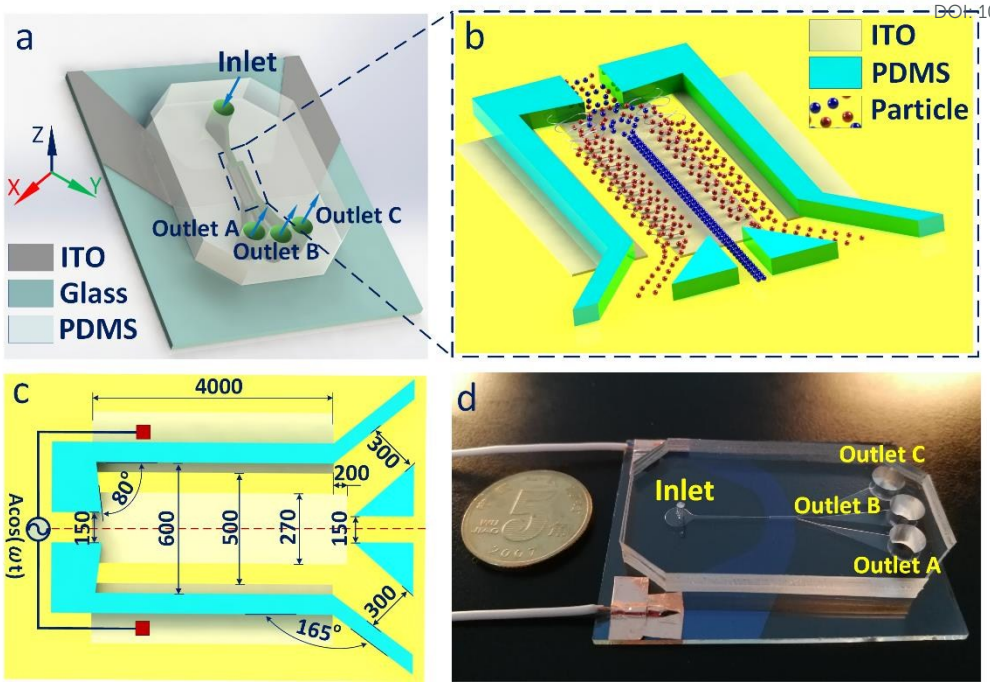

Fig. 1 Schematic diagrams and image of ICEO particle separation device: **a** Three-dimensional view of the experimental setup, **b** Illustration of ICEO particle separation principle, **c** Configuration of the ITO-based electrode and PDMS-based channel (all lengths are in microns), **d** Photograph of the device.

recorded using a high-speed CCD camera (DP27, Olympus, Japan). Before performing each experiment, the internal structure of the closed channel was given a hydrophilic treatment in a plasma machine and soaked with Tween 20 solution to slow down the adhesion of particles and cells. Buffer solution containing particles or cells was infused into the microchannel through a 10-mL glass syringe using an automated syringe pump (Harvard Apparatus 70-4501). The AC signal applied to the driving electrode was generated by a function generator (TGA12104), magnified by an amplifier (TEGAM) and monitored by an oscilloscope (TDS2024, Tekronix, USA). Scanning electron microscopy (SEM) (HITACHI, SU8010) was applied to obtain the images of samples in the isolation of nanoparticles.

Preparation of cell and particle samples.

To prepare the yeast cells, 100 mg of dry yeast cells were revived and cultured in 50-mL of DI water at 50 °C for 2 h. To obtain relatively pure yeast cells, we pipetted a 2-mL cultured yeast solution for further processing. The solution was placed in a centrifuge (TGL-16B) for 30 s, after which the culture solution was replaced by KCl solution with a conductivity of 10 μS/cm. The yeast cells in the KCl solution were then washed and resuspended by performing an ultrasonic treatment for 30 s. This procedure was repeated six times.

Beads of 4-μm silica, 2-μm and 5-μm polystyrene (PS), and 4-μm PMMA were purchased from Sigma-Aldrich, (USA). 500-nm fluorescent PS beads were purchased from BangsLabs, Inc. (USA). The beads were washed in KCl solution after centrifuging at 3000 r/min for 5 minutes, forming a 2-ml particle sample solution.

Results and Discussion

ICEO-based device for particle separation.

The protocol for particle separation via ICEO vortices is shown schematically in Fig. 1a, b. By adjusting the over-potential on the electric double layer, the operation of the device is based on whether the particles are trapped in or escaping from the ICEO vortices. Particles with different physical properties, such as density, size, and shape, exhibit different behaviours in a given vortex. Particles with negligible inertia in the ICEO vortices tend to move inward and therefore are trapped near the vortex core; particles with non-negligible inertia tend to spiral outward and therefore escape being focused in the FSL of the vortex pairs.

In the present experiments, ICEO vortex pairs are generated on the ITO-based floating electrode, the profile of which is precisely and flexibly controlled by adjusting the AC voltage applied to the left and right driving electrodes. A PDMS-based micro-channel was designed to direct the flow, and the behaviours of particles within the channel are then observed. Moreover, the ITO-based electrodes and PDMS-based channel were fabricated by standard soft lithography and integrated employing plasma-bonding technology. The specific dimensions employed in the device are shown in Fig. 1c. Details of the processing steps have been given in previous reports[10, 17]. A photograph of the actual device is shown in Fig. 1d. The experiment begins by pumping the mixture from the inlet into a narrow, straight channel. By applying an AC signal Φ=Acos(ωt) on the left driving electrode and grounding the right driving

View Article Online
DOI: 10.1039/C8NR09148J

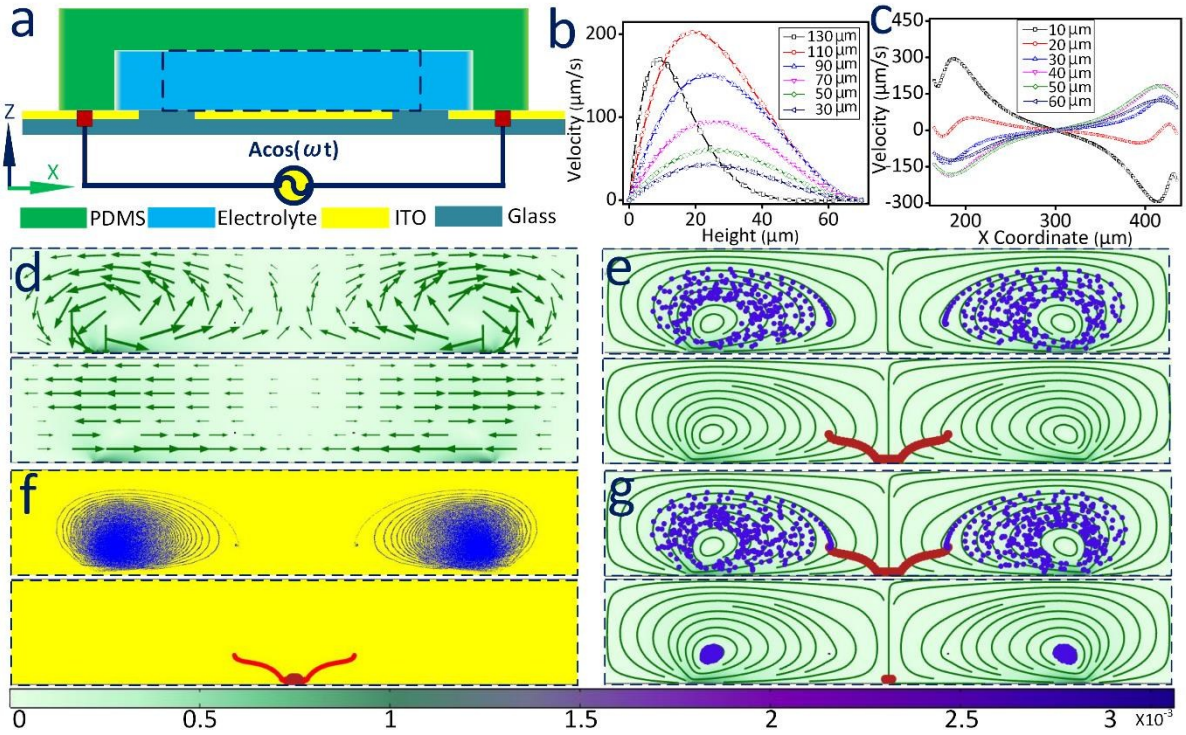

Fig. 2 Simulation model and numerical results at A=7.5 V f=150 Hz: **a** Schematic of the configured model; **b** Vertical velocities along the cutting lines (parallel to the Z coordinate) at distances 30, 50, 70, 90, 110, and 130 μm from the centerline; **c** Transverse velocities along the cutting lines (parallel to the X coordinate) at distance 10, 20, 30, 40, 50, and 60 μm from the channel bottom; **d** Distributions of the vortices and transverse flow fields; **e** Simulations illustrating vortex trapping of PS5 particles, and silica micro-beads escaping from vortices; **f** simulations showing trajectories and final state of the PS5 and silica micro-beads; **g** simulations depicting the separation of PS5 and silica particles. To better view the simulation results, we only chose the area outlined by the blue dashed rectangle in (a) (Movie 1) (The boundary conditions of the numerical simulation are given in the section 1 of the Supporting Information).

electrode, controllable symmetrical ICEO vortices are formed on the floating electrode. Under a specific vortex profile, particles with high inertia escape from the vortices, are concentrated at the FSL, and flow into outlet B, whereas particles with low inertia are trapped and move toward the vortex cores, being focused therefore on the periphery of the floating electrode and ending up in outlets A and C.

Working mechanism of ICEO-based particle separation.

We configured a numerical model to explore the ICEO micro-stream distribution and particle separation. The designed two dimensional (2D) model (Fig. 2a) consists of a PDMS channel with a rectangular cross section, an electrolyte domain, and three ITO electrodes (left and right driving electrodes, and a middle floating electrode) located in a glass substrate. In this 2D model, assuming the salt concentration is homogeneous, the reduced Laplace equation can be solved to obtain the electric field in the electrolyte by considering the electrolyte/electrode interface as a surface capacitor. By combining the electric field and Helmholtz–Smoluchowski formula for the electro-osmotic slip, the ICEO slip velocity on the floating electrode is derived. We substituted the ICEO slip velocity into the Navier–Stokes equation for a low Reynolds number flow to describe the micro-stream in the channel. Plots of the vertical and transverse velocity distributions are given in Fig. 2b and c. The vortex distribution and transverse flow field at different levels are exhibited in Fig. 2d. The total force exerted on the particles in the ICEO vortices stems from the gravitational field, the fluid, and electric field, and given by[19, 27]

$$F_i = m_p g_i + \iint \sigma_{ij} n_j dS + \sum \sigma_q \Delta S E \quad 1, 2.....d \qquad (1)$$

where g_i is the gravitational acceleration, σ_{ij} the fluid stress tensor on the sphere, σ_q the surface charge density, and d the dimensionality of the flow; here we concentrate on 2D flow. The effect from the fluid and electric field can be approximately evaluated to yield the important force in the equation of motion for the particles in the ICEO vortices[28],

$$F_i = 6\pi a\mu \left(v_i - u_i\right) + \left(m_p - m_f\right) g_i + F_i^{DEP} \qquad (2)$$

The terms from left to right are the Stokes drag, which is proportional to the difference between the particle velocity v_i and the flow velocity u_i, the buoyancy force, which is proportional to the difference between the particle mass m_p and the fluid mass m_f having the same volume as the particles, and the dielectrophoretic force of the particles.

View Article Online
DOI: 10.1039/C8NR09148J

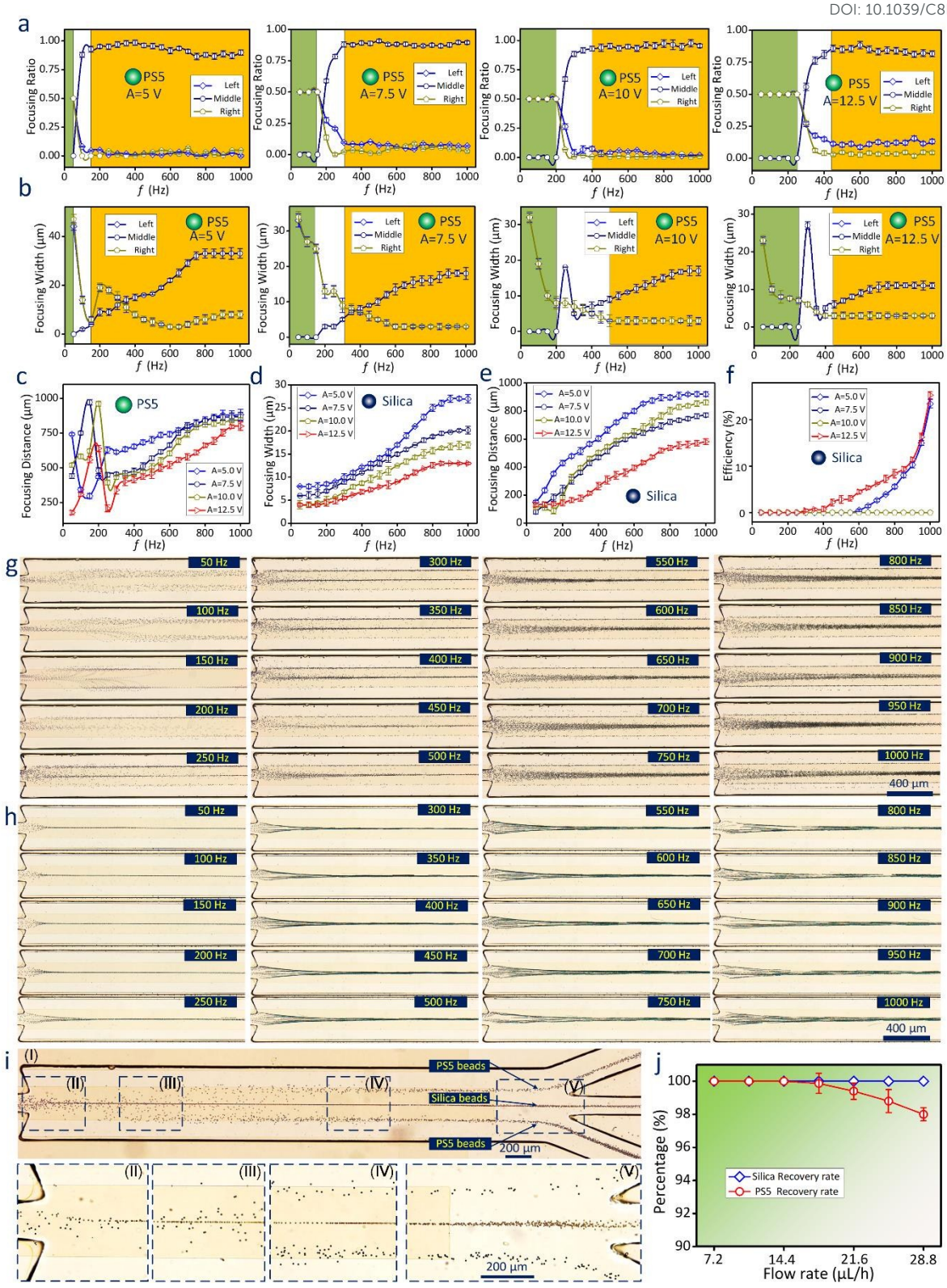

Fig. 3 Separation experiment results for PS5 and silica micro-beads validating our method. **a**–**c** Focusing characterizations of PS5 micro-beads. **a**, **b** Frequency dependence of focusing ratio and focusing width of PS5 micro-beads (The green/orange backgrounds indicate the frequency ranges that almost all PS5 micro-beads are focused at the both sides/center of the floating electrode). **c** Focusing distance versus frequency of PS5 micro-beads for different voltage intensities. **d**–**f** Focusing characterizations of silica particles. **g** Transferring of the PS5 micro-bead trapping position from both sides to the middle of the floating electrode for frequencies from f=50 Hz to f=1000 Hz. **h** Focusing position of silica particles always locating in the centerline of the floating electrode at all the frequency domain. **i** Experimental demonstration of particle separation at A=7.5 V, f=150 Hz. **j** Separation efficiency against flow rate.

View Article Online
DOI: 10.1039/C8NR08146A

Given u_i and E_i, particle trajectories can be predicted. Fig. 2e depicts the behaviours of micro-beads of PS5 (in blue) and silica (in red) in the ICEO vortices at A=7.5 V and f=150 Hz. The PS5 particles are seen to move together with the vortex pair. Because the attractors at the vortex cores are produced through a successive joint action of the gravitational and DEP forces, the PS5 particles progressively move toward the vortex cores and finally where they are concentrated. In contrast, silica particles are not captured and escape from ICEO vortices. Under the counteraction of the gravitational and upward hydrodynamic forces, silica particles are suspended near the floating electrode. Electro-osmotic flows pointing to the central line of the floating electrode push silica particles toward the FSL. As a result, silica particles are focused into a slender particle stream. From their trajectories in the vortices (Fig. 2f), the PS5 and silica micro-beads exhibit different focusing behaviours in the ICEO vortices, being trapped at the two vortex cores and at the FSL, respectively. With typically different focusing characterizations in the ICEO vortices, we analysed the separation performances by releasing PS5 and silica micro-beads from a location 40 µm away from the central line and 20 µm from the bottom. As expected, all the silica particles are focused at the FSL, whereas the PS5 particles are trapped on both sides of the floating electrode (Fig. 2g).

Experimental verification of this method.

We performed a series of experiments to verify this method in separating particles using different physical properties. PS5 breads and 4-µm-diameter silica particles were used as separation targets. We first studied the frequency dependence of particle focusing characterizations at different voltage intensities. Three indexes were defined to depict the particle focusing characterizations, including focusing ratio, focusing width, and focusing distance. Focusing ratio can be calculated by the formula:

$$R = N_f / N_a \quad (3)$$

where, N_f is the number of particles focused in the particle stream; N_a is the number of all the particles entering the device. Focusing width demonstrates the width of particle stream when the particle focusing reaches the steady state. Focusing distance is the distance from the entrance of the separation region to the position that the focusing width becomes a constant value. Schematic diagram defining the focusing width and focusing distance is given in Fig. S1. Fig. 3a and b show the relationship between the voltage intensity input and particle-focusing performance (focusing ratio and focusing width, respectively) for PS5 micro-beads. When the frequency ranges from 50 to 200 Hz (indicated by the green backgrounds) at A=10 V, all the PS5 particles are focused at the left and right sides of the floating electrode (Fig 3a), and their focusing widths decrease from 32.01 to 7.12 µm (Fig 3b). In the frequency range of 400-1000 Hz (denoted by the orange backgrounds) at A=10 V, almost all the PS5 particles are focused at the center of the floating electrode (Fig 3a), and the focusing width increases from 7.21 to 17.13 µm (Fig 3b). With different voltage intensities, the PS5 beads gave similar trends in performance. In the frequency ranges indicated by the green backgrounds, the focusing ratio of PS5 particles was maintained at 100% at the left and right edges of the floating electrode, whereas no silica particles were focused at these two positions. In contrast, other frequency inputs (denoted by the orange backgrounds) resulted in nearly a 100% focusing ratio for PS5 and silica micro-beads along the central line of the floating electrode. Fig. 3c plots the relationship between focusing distance and frequency input for PS5 micro-beads. With increasing voltage frequency, the particle stream widths increase along the two side walls but decrease along the central line. The frequency dependence of both focusing width and distance for silica breads are given in Fig. 3d and e, respectively. Note that both particles reach a steady state within a distance of 1000 µm. At frequencies between 50–1000 Hz, no PS5 beads had escaped from the floating electrode whereas some silica particles had; the escaping efficiency versus frequency is shown in Fig. 3f. Image sequences demonstrating the focusing characteristic versus frequency for PS5 and silica micro-beads at A=7.5 V are given in Fig. 3g and h, respectively.

Given the focusing characterizations of PS5 and silica micro-beads, we investigated the separation capability of our method. When no AC voltage is employed, PS5 and silica particles are randomly distributed in the channel and flow toward outlets A, B, and C. Once the voltage was applied with A=7.5 V and f=150 Hz, a clear separation between PS5 and silica micro-beads was observed (Movie 2). PS5 beads were trapped by the ICEO vortices and moved towards the vortex cores. They were focused into a particle stream and moved along both sides of the floating electrode. Silica particles however escaped from the vortices and were drawn towards the straight FSL. Under the successive action of ICEO vortex pairs, these particles were focused into a fine particle stream and moved along the central line of the floating electrode. From micro-images (using a 4× objective) and magnified images (using a 10× objective) of the separation process (Fig. 3i), PS5 micro-beads are seen to be directed to outlets A and C, whereas silica particles are diverted to outlet B.

The flow rate has a significant effect on the separation performance. For this, we also studied the relationship between the separation efficiency and fluid flow (Fig. 3j). We found that efficiency always remains capped at 97% when the fluid flow ranges from 7.2 µL/h to 28.8 µL/h.

Density-based and size-based particle separations.

We have demonstrated that this method enables micro-particle separations based on physical properties. However, to further explore the capabilities of this method, we first fine-tuned the input voltage and flow rate to separate particles of different densities but the same diameter. For this purpose, 4-µm-diameter beads of PMMA and silica were used. The working mechanism behind density-based particle separation of the device is illustrated in Fig. 4a. A three-dimensional numerical simulation indicated that the PMMA particles are extracted by the vortices and move around the two vortex cores, whereas silica particles escape from the vortex pairs and move towards the symmetry axis of the bipolar electrode. Moreover, by analysing sequential cross-section simulations (Fig. 4b), the PMMA particles flowing through the micro-channel experience a negative DEP force. It is this force that contributes to the

View Article Online
DOI: 10.1039/C8NR09148J

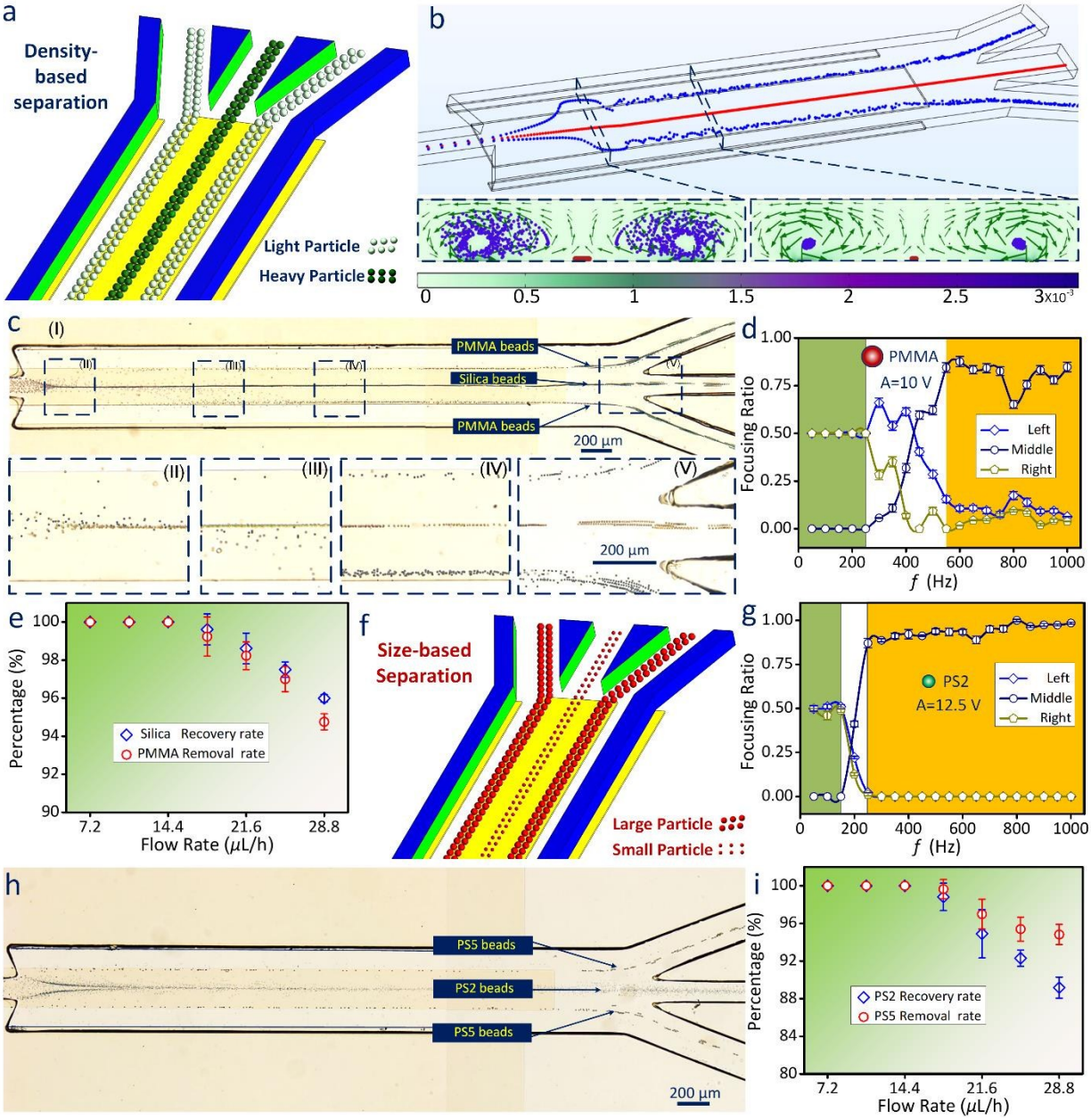

Fig. 4 Performance of this method for density-based and size-based separation. **a** Schematic illustrating density-based separation. **b** Three-dimensional ICEO-based separation simulation and particle state in different cross sections at f=200 Hz, A=10 V. **c** The actual microscope images demonstrating the density-based separation under 4× and 10× objectives at A=10 V, f=200 Hz. **d** The frequency dependency of focusing ratio of PMMA particles at A=10 V f=200 Hz. **e** Particle separation performance when varying the flow rate at f=200 Hz, A=10 V. **f** Illustration of size-based separation. **g** The dependence of focusing ratio of PS2 particles on frequency (The green/orange backgrounds indicate the frequency ranges that almost all the PMMA or PS2 micro-beads are focused at the both sides/center of the floating electrode). **h** Experimental demonstration of separation of PS5 and PS2 micro-beads at A=12.5 V, f=250 Hz. **i** Flow-rate dependence of performance in size-based separation.

centripetal movement of the PS5 micro-beads. By passing the particles through the same vortex continuously, the separation distance is further amplified, resulting in a significant difference in trajectories. The consequent separation (Fig. 4c) is in line with numerical results (Fig. 4b). Before applying the AC signal to the driving electrode, all particles flowed randomly toward outlets A, B, and C. Under the voltage and frequency settings of A=10 V and f=200 Hz, a clear separation between PMMA particles and silica particles was evident (Movie 3). The PMMA particle stream was directed towards outlets A and C, whereas silica particles went through outlet B. Under a practical voltage input (f=200 Hz, A=10 V) and fluid flow (u=18 μL/h), almost all the PMMA particles were trapped by the ICEO vortices and focused along the two sides of the floating electrode when subjected to the frequencies indicated by the green backgrounds, whereas the majority of PMMA particles escaped from the vortex pairs

View Article Online
DOI: 10.1039/C8NR09148J

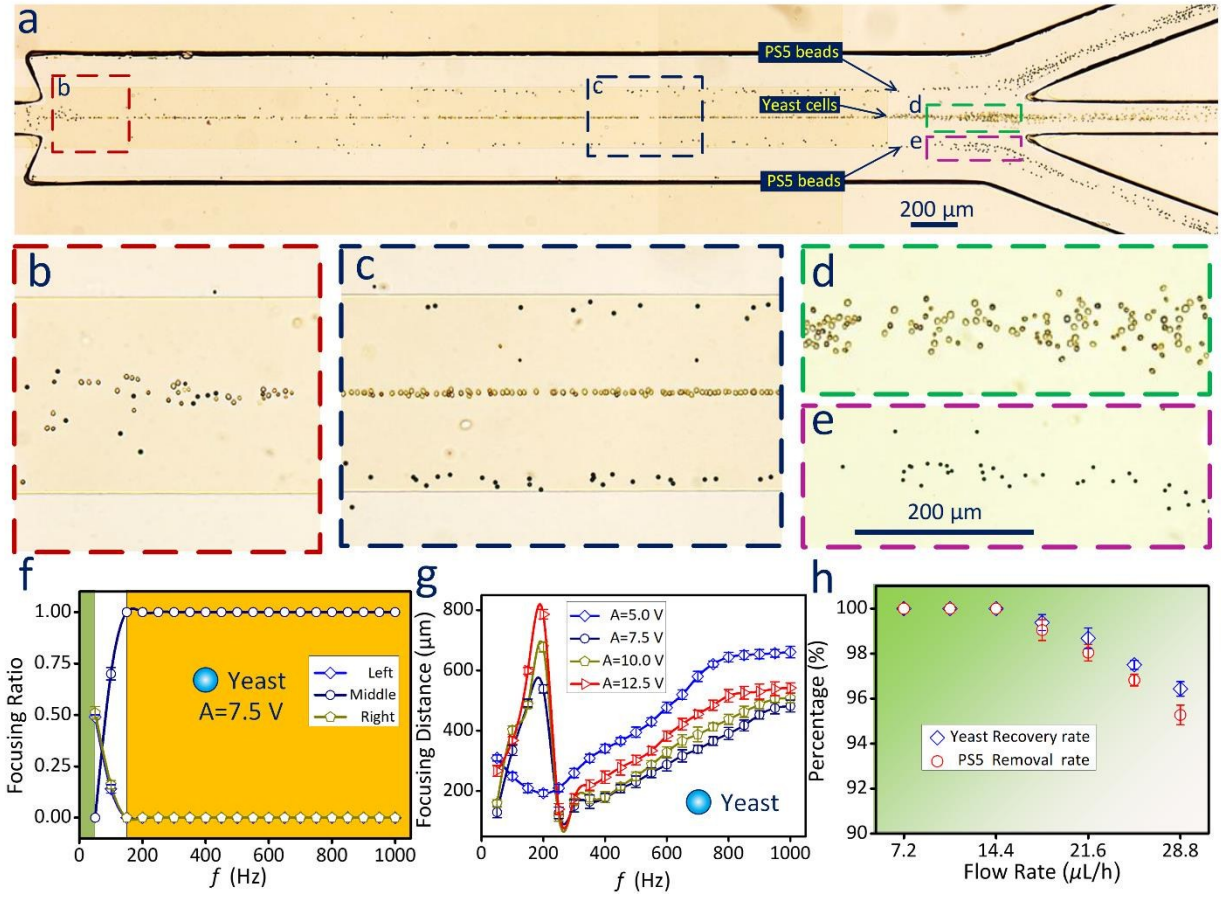

Fig. 5 Cell purification. **a** Actual image illustrating the purification process of yeast cells at A=7.5 V f=150 Hz. **b–e** Zoomed-in photographs of the location defined in a. **f, g** The plots of focusing ratio and focusing distance against frequency input, respectively (The green/orange background indicates the frequency range that almost all the yeast cells are focused at the both sides/center of the floating electrode). **h** The purification performance under different flow rate.

and were concentrated at the FSL at the frequencies denoted by the orange backgrounds (Fig. 4d and Fig. S2). Fig. 4e shows the relationship between the fluid flow and particle-separation performance for PMMA and silica micro-beads. When the flow rate is below 14.4 μL/h, the removal rate of PMMA particles and the recovery rate of silica particles were 100% without deviation. A rise in fluid flow rate to 28.8 μL/h resulted in a 96% recovery rate of silica particles and a 95% removal rate of PMMA particles. After validating capability of this method in density-based separation, we then exploited the potential of this method in size-based particle separation (see schematic in Fig. 4f). Prior to conducting separation experiment, we also explored the ICEO focusing characteristics of 2-μm-diameter PS (PS2) beads; a plot of the focusing ratio against input frequency with A=12.5 V is shown in Fig. 4g. The other focusing characterizations of PS2 particles are shown in Fig. S3. Fig. 4h gives an optical image illustrating the separation process of PS2 and PS5 particles with settings of f=250 Hz, A=12.5 V, and u=18 μL/h. Note that the smaller PS2 particles overcome the vortex traps and escape to the FSL whereas the bigger PS5 particles are focused towards the two sides of the floating electrode. One reasonable explanation for this interesting phenomenon may be that the attractive force between the ions on the polarized particles and in the EDL may play a significant role in the separation of the smaller particle[29]. Under the combined effect of the attractive force and vortex drag, the PS2 particles are focused towards the FSL, whereas PS5 particles exhibit a spiralling motion around the vortex cores (Movie 4). A negative DEP force near both sides of the bipolar electrode elevate the PS5 particles towards the vortex cores, thereby reducing the closed orbit of particles and narrowing the two particle streams. The separation performances under different flow rates (Fig. 4i) show that at low flow rates, ranging from 7.2 to 14.4 μL/h, the removal rate of PMMA particles and recovery rate of silica particles are maintained at 100%. In contrast, at the higher flow rate of 28.8 μL/h, the recovery rate of PS5 particles and the removal rate of PS2 particles decrease to 94% and 88%, respectively.

After a full demonstration of the density-based and size-based separation with a sample throughput of 7.2–28.8 μL/h, we investigated the recovery of yeast cells in a mixture (Movie 5). We first examined the ICEO-based focusing performance of yeast cells. Almost all cells were captured by the vortex pairs at relatively low frequency, whereas all the cells are focused into a cell stream at the FSL at relatively high frequency. Fig. 5a

View Article Online
DOI: 10.1039/C8NR09148J

presents an image of the entire purification process for yeast cells with settings A=7.5 V and f=150 Hz. The magnified images

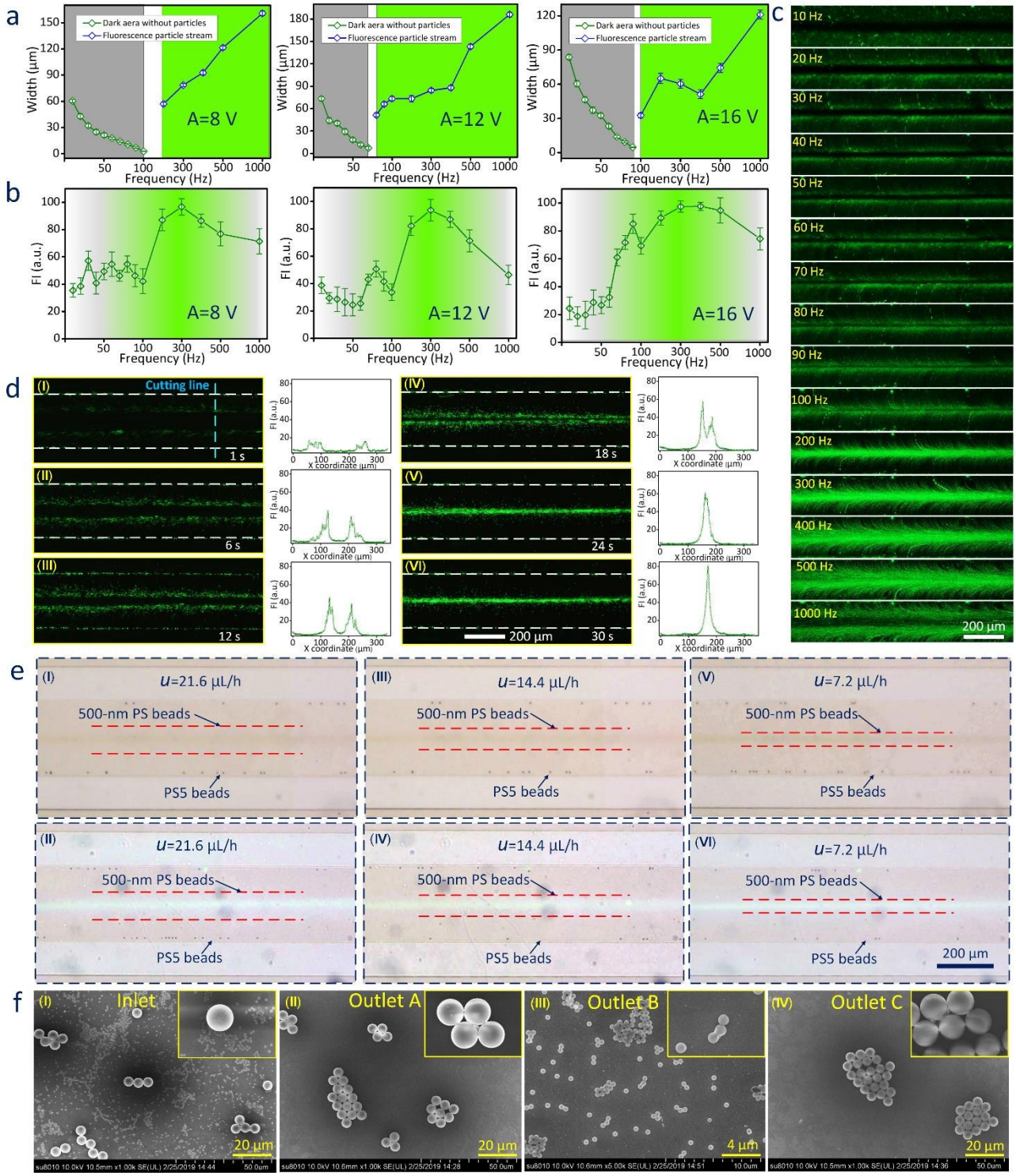

Fig. 6 Separation of nanoparticles and microparticles: **a, b** Plots of nanoparticle focusing widths and fluorescence intensity (FI) of the 500-nm fluorescent PS beads at A=8, 12, 16 V (The gray/green backgrounds indicate the frequency ranges that almost all the nanoparticles are focused at the both sides/center of the floating electrode); **c** An image sequence illustrating the dependence of the ICEO characteristic on voltage frequency at A=12 V; **d** Images of the dynamic motion of 500-nm fluorescent PS particles along with corresponding graphs illustrating FI against cutting line; **e** Micrographs demonstrating the separation of 500-nm and 5-μm PS particles at f=200 Hz, A=12 V for different flow rates; **f** SEM images of the original sample and the separated samples.

(Fig. 5b, c, d, and e) of the locations defined in Fig. 5a are recorded under the 10× objective and identify the behaviours of yeast cells and PS5 beads in the purification process. The plots of focusing characterizations of yeast cells against

View Article Online
DOI: 10.1039/C8NR09148J

frequency input (Fig. 5f, g, and Fig. S4) show that with increasing voltage frequency, the trapping location of the yeast cells switches from both sides to the central line of the floating electrode. Under the ICEO vortex action, yeast cells escape from the vortices and are transported to the FSL, whereas the foreign constituents, the PS5 beads, are drawn into the vortices and move around the two vortex cores, enabling its stable trapping. We also exploited the effect of throughput on cell purification performance. The relationship between flow rate and cell-separation performance is plotted in Fig. 5h.

ICEO characterization and isolation of nanoparticles.

The isolation of nanoscale exosomes from microscale blood cells plays a significant role in health monitoring, disease diagnoses and so on[2, 3, 30, 31]. Besides, obtaining graphene oxide sheet with precise size (microscale or nanoscale) from initial resultants is also a significant process in drug delivery and solar cell fabrication[5, 6]. In these regards, we also explored the capability of our method by separating 500-nm fluorescent and PS5 particles. Prior to separation, we first investigated the ICEO characterization of nanoparticles. Similar to microscale particles, nanoparticles may be captured by the ICEO vortices and move as vortices in spiral trajectories at the frequencies indicated by the gray backgrounds, leading to a dark area without nanoparticles around the FSL (Fig. 6a and b). Within this frequency interval, the dark area is reduced and fluorescent intensity (FI) is weakened gradually with increasing frequency (Movie 6). The mechanism behind this phenomenon is associated with the escape of nanoparticles from the vortices, leading to a widening of the closed orbit.[32] By increasing the voltage frequency to the ranges denoted by the green backgrounds, nanoparticles begin to escape from the vortices and move towards the FSL. As a consequence, a bright fluorescent nanoparticle stream begins to light up the dark FSL (Fig. 6a and b). Notably, nanoparticles are focused into a fine particle stream at the straight FSL near the relaxation frequency of 200 Hz for the floating electrode[17]. When the frequency is further increased, the nanoparticles in the stream disperse, resulting in a broad stream and weaker FI (Fig. 6a and b). The frequency dependence of the nanoparticles in the ICEO vortices at A=12 V is given in a sequence of images (Fig. 6c). The dynamic motion in nanoparticle focusing is given in Fig. 6d for the setting f=200 Hz and A=12 V. Once the input voltage is applied, the nanoparticles are pushed towards the FSL. During focusing, nanoparticles are increasingly concentrated, giving rise to a brighter particle stream. Along with each image, plots of the FI observed along the cutting line are shown to highlight further the focusing process of fluorescent nanoparticles. After a 30-s focusing period, almost all the nanoparticles are pushed towards the FSL, giving rise to a slender and bright particle stream.

On the basis of the nanoparticle ICEO characterization, we separated 500-nm and 5-μm PS particles with f=200 Hz and A=12 V, and exploited the dependence of the separation performance on flow rate. Bright-field and corresponding fluorescence images (Fig. 6e) illustrate the resultant separation at different flow rates. To observe clearly the separation performance for fluorescent nanoparticles and microparticles simultaneously, we used ultraviolet light from beneath the device to excite the fluorescent nanoparticles in the bright field. Although nanoparticles are isolated from the mixture at u=21.6 μL/h, some free nanoparticles were not focused into the particle stream (Movie 6). By reducing the flow rate to 14.4 μL/h, nanoparticle leakage was addressed to some extent. If the flow rate is decreased to 7.2 μL/h, the nanoparticles are concentrated into a narrow particle stream, attaining then an ideal separation performance. Moreover, SEM images of the original sample (from inlet) and the separated samples (from outlets A, B, and C) at u=7.2 μL/h are presented in Fig. 6f to confirm particle sizes.

Conclusions

In this work, we put forward a direct method of micro/nano particle separation based on ICEO vortices in continuous flow. Theoretically, we first explored the performance of particles in the ICEO vortices. In a specific ICEO vortex profile, light particles were trapped and move around the vortex cores driven by the Stokes force. Two non-ignorable forces, DEP force near the edge of the floating electrode and the gravitational force, established a lowest point in the spiral motion driving the particle towards the vortex cores. Consequently, these particles were confined to two fine particle streams. Furthermore, the focusing location can be flexibly switched from the central line to both sides of the floating electrode by adjusting the input voltage intensity and frequency. Unlike light particles, heavy particles escaped from these ICEO vortices as the vortices appeared weak in overcoming the downward gravitational force of these particles and made them move with the vortices. The symmetric electro-osmotic flows near the floating electrode surface pushed these particles towards the FSL. After the successive action of the ICEO vortices, heavy particles were focused into a narrow particle stream at the FSL.

We demonstrated the wide applicability of this method to various target particles through a variety of separation tests considering the combined effect of sample size and density. First, we separated PS5 and silica micro-beads to validate our method and our simulation model. The separation efficiency approached 100% and the experimental results were in line with our simulations. Second, we separated PMMA and silica beads with the same diameter of 4 μm to exploit the potential for density-based separation; a separation efficiency above 99% was achieved. Third, we also studied size-based separation with a separation efficiency exceeding 98%.

We exploited our method to purify yeast cells from impeding particles, obtaining a recovery rate exceeding 96% with flow rates ranging from 7.2 to 28.8 μL/h. The weak voltage intensity and sustained vortex action provided the gentle and contact-free condition for cell manipulation.

Our method also performed well in isolating nanoparticles. Similar to the ICEO focusing characteristics of micro-beads, nanoparticles can be captured by vortices and focused into two particle streams along both sides of the floating electrode with

low frequency voltages, whereas they escaped from vortices and concentrated into a particle stream at the FSL under relatively high frequencies. Depending on the ICEO focusing characteristics of nanoparticles in experiment, we explored the capacity to isolate nanoparticles from mixtures and attained good separation.

In addition, the chip structure and operation are simple. Only particle samples are injected into the channel, and the particles are directed to a designed outlet under the successive action of ICEO vortices without peripheral equipment and complicated operations. This method will be a promising candidate for micro/nano particle separation.

Conflicts of interest

There are no conflicts to declare

Acknowledgements

This work is supported by the National Natural Science Foundation of China (No. 11672095, 11872165 and 11802078); Self-Planned Task (SKLRS201803B) of State Key Laboratory of Robotics and System (HIT); Opening fund of State Key Laboratory of Nonlinear Mechanics.

Notes and references

1. H. Shafiee, M. B. Sano, E. A. Henslee, J. L. Caldwell and R. V. Davalos, *Lab on a chip*, 2010, **10**, 438-445.
2. M. Wu, Y. Ouyang, Z. Wang, R. Zhang, P. H. Huang, C. Chen, H. Li, P. Li, D. Quinn, M. Dao, S. Suresh, Y. Sadovsky and T. J. Huang, *Proceedings of the National Academy of Sciences of the United States of America*, 2017, **114**, 10584-10589.
3. M. An, J. Wu, J. Zhu and D. M. Lubman, *Journal of proteome research*, 2018, DOI: 10.1021/acs.jproteome.8b00479.
4. P. Li, Z. Mao, Z. Peng, L. Zhou, Y. Chen, PH. Huang, CI. Truica, JJ. Drabick, WS. El-Deiry, M. Dao, S. Suresh, TJ. Huang, *Proceedings of the National Academy of Sciences of the United States of America*, 2015, **16**, 4970–4975.
5. C. Cui, J. Huang, J. Huang and G. Chen, *Electrochimica Acta*, 2017, **258**, 793-799.
6. Q. Du, C. Liu and X. Wang, *Journal of Computational Physics*, 2006, **212**, 757-777.
7. J. K. Lim, D. C. Chieh, S. A. Jalak, P. Y. Toh, N. H. Yasin, B. W. Ng and A. L. Ahmad, *Small*, 2012, **8**, 1683-1692.
8. Y. Zhu, H. Wang, K. Wan, J. Guo, C. He, Y. Yu, L. Zhao, Y. Zhang, J. Lv, L. Shi, R. Jin, X. Zhang, X. Shi, and Z. Tang, *Angew. Chem. Int. Ed*. 2018, **57**, 9059 –9063.
9. M. Wu, Z. Mao, K. Chen, H. Bachman, Y. Chen, J. Rufo, L. Ren, P. Li, L. Wang and T. J. Huang, *Advanced functional materials*, 2017, **27**.
10. X. Chen, Y. Ren, W. Liu, X. Feng, Y. Jia, Y. Tao and H. Jiang, *Analytical chemistry*, 2017, **89**, 9583-9592.
11. N. Lewpiriyawong, K. Kandaswamy, C. Yang, V. Ivanov and R. Stocker, *Analytical chemistry*, 2011, **83**, 9579-9585.
12. X. Hu, P. H. Bessette, J. Qian, C. D. Meinhart, P. S. Daugherty and H. T. Soh, *Proceedings of the National Academy of Sciences of the United States of America*, 2005, **102**, 15757-15761.
13. CT. Yavuz, JT. Mayo, WW. Yu, A. Prakash, C. Joshua, JC Falkner, S. Yean, L. Cong, HJ. Shipley, A. Kan, M. Tomson, D. Natelson, LC. Vicki, Science, 2006, **314**, 964-967.
14. SB. Kim, SY. Yoon, HJ. Sung, SS. Kim, Analytical chemistry, 2008, **80**, 2628-2630
15. A. A. Kayani, K. Khoshmanesh, S. A. Ward, A. Mitchell and K. Kalantar-Zadeh, *Biomicrofluidics*, 2012, **6**, 31501.
16. P. Arosio, T. Muller, L. Mahadevan and T. P. Knowles, Nano letters, 2014, 14, 2365-2371.17. Y. Ren, W. Liu, Y. Jia, Y. Tao, J. Shao, Y. Ding and H. Jiang, *Lab on a chip*, 2015, **15**, 2181-2191.
18. RD. Vilela, AE. Motter, Physical review letters, 2007, **99**, 264101.
19. I. J. Benczik, Z. Toroczkai and T. Tel, *Physical review letters*, 2002, **89**, 164501.
20. M. Z. Bazant and T. M. Squires, *Physical review letters*, 2004, **92**, 066101.
21. I. Lazo, C. Peng, J. Xiang, S. V. Shiyanovskii and O. D. Lavrentovich, *Nature communications*, 2014, **5**, 5033.
22. T. M. Squires and M. Z. Bazant, *Journal of Fluid Mechanics*, 2004, **509**, 217-252.
23. Y. Ren, J. Liu, W. Liu, Q. Lang, Y. Tao, Q. Hu, L. Hou and H. Jiang, *Lab on a chip*, 2016, **16**, 2803-2812.
24. Y. Wu, Y. Ren, Y. Tao, L. Hou and H. Jiang, *Analytical chemistry*, 2016, **88**, 11791-11798.
25. W. Liu, J. Shao, Y. Ren, J. Liu, Y. Tao, H. Jiang and Y. Ding, *Biomicrofluidics*, 2016, **10**, 034105.
26. Y. Jia, Y. Ren and H. Jiang, *RSC Advances*, 2015, **5**, 66602-66610.
27. E. Balkovsky, G. Falkovich and A. Fouxon, *Physical review letters*, 2001, **86**, 2790-2793.
28. Y. Ren, X. Liu, W. Liu, Y. Tao, Y. Jia, L. Hou, W. Li and H. Jiang, *Electrophoresis*, 2018, **39**, 597-607.
29. TP. Albert, B. Rolf, N. Willem, JB. Henk, Surface Science Reports, 2002, **47** 1-32.
30. D. Ding, D. Wang, M. Zhao, J. Lv, H. Jiang, C. Lu and Z. Tang, *Advanced materials*, 2017, **29**.
31. M. Zhao, F. Yang, C. Liang, D. Wang, D. Ding, J. Lv, J. Zhang, W. Hu, C. Lu and Z. Tang, *Advanced Functional Materials*, 2016, **26**, 5182-5188.
32. J.-R. Angilella, R. D. Vilela and A. E. Motter, *Journal of Fluid Mechanics*, 2014, **744**, 183-216.

View Article Online
DOI: 10.1039/C8NR09148J

We present a direct particle separation method based on induced charge electro-osmotic vortices in continuous flow.